

# Path-integral Monte-Carlo simulations for electronic dynamics on molecular chains:

## II. Transport across impurities

Lothar Mühlbacher<sup>1\*</sup> and Joachim Ankerhold<sup>1,2</sup>

*1: Physikalisches Institut, Albert-Ludwigs-Universität, D-79104 Freiburg, Germany and*

*2: Service de Physique de l'Etat Condensé, Centre d'Etudes de Saclay, 91191 Gif-sur-Yvette, France*

(Dated: Date: October 7, 2021)

Electron transfer (ET) across molecular chains including an impurity is studied based on a recently improved real-time path integral Monte Carlo (PIMC) approach [J. Chem. Phys. **121**, 12696 (2004)]. The reduced electronic dynamics is studied for various bridge lengths and defect site energies. By determining intersite hopping rates from PIMC simulations up to moderate times, the relaxation process in the extreme long time limit is captured within a sequential transfer model. The total transfer rate is extracted and shown to be enhanced for certain defect site energies. Further, it is revealed that the entire bridge compound approaches a steady state on a much shorter time scale than that related to the total transfer which allows for a simplified description of ET along donor-bridge-acceptor systems in the long time range.

### I. INTRODUCTION

Charge transfer in native or designed molecular structures has attracted a substantial amount of research recently [1, 2, 3, 4, 5]. This is mostly due to the perspective to exploit corresponding processes in a controlled way in integrated nano-electrical circuits [6, 7]. However, even though tremendous progress has been achieved, still various rather fundamental questions need to be elucidated. Certainly, one of these is the role of the environmental degrees of freedom, originating from solvent and/or residual vibronic molecular degrees of freedom, which are often neglected in approaches based on transport theories for clean mesoscopic devices. Nevertheless, they are known to be crucial for charge transfer in condensed phase structures [4, 8, 9]. This is assumed to be particularly true in cases where impurities along the transport channel are to be surmounted by an intimate interplay between charge-phonon interactions such as thermal activation, nuclear tunneling, and coherent electronic tunneling (superexchange).

The development of effective approaches to include complex environments in the quantum dynamics of electronic systems has been one of the major goals in chemistry and physics as well [10]. The widely used and powerful Redfield formulation has revealed important aspects of charge transfer in various systems [11, 12, 13, 14]. However, as an approximate method it is limited to weak friction with high frequency vibronic modes and sufficiently high temperatures. In a previous paper [15], referred to as Ref. [I] henceforth, we used a numerically exact Monte Carlo path integral approach (PIMC) to capture electronic transfer (ET) dynamics in donor-bridge-acceptor (DBA) systems. In essence, it exploits that the path integral formulation allows for an exact elimination of the bath as well as the quasi-classical elec-

tronic degrees of freedom which reduces the dimensionality of the Hilbert space considerably [16]. The method has the merit of being applicable in the whole parameter space, that is also in those ranges where approximate methods fail, e.g. for low frequency environments and low temperatures. It further allows to treat bridges with a larger number of electronic sites and up to sufficiently long times so that in Ref. [I] we could investigate the length dependence of the total transfer rate from donor to acceptor, which has also been the subject of recent experiments [17, 18, 19].

In Ref. [I] we paid particular attention to charge diffusion across a DBA complex with energetically degenerated bridge states. Here, we continue this study by analysing the impact of an impurity located in the center of the bridge. One may expect that the existence of a defect is the typical situation in native degenerated structures. Moreover, meanwhile advanced chemical synthesis allow to “dope” molecular chains in a controlled way and study transport properties by linking them to external leads [20]. The archetypical case is thereby that of a defect with an energy gap to its surrounding electronic sites as this scenario includes effectively also defects in the electronic intersite coupling. Our main focus here lies on a microscopic description of the transport *dynamics* and the total transfer rate, which for isolated DBA systems corresponds to the relaxation rate towards thermal equilibrium, and for integrated DBA structures subject to a dc-voltage is related to the steady state flux [4]. In general, the long time limit where a global thermal equilibrium state is established, cannot be reached within typical times accessible in PIMC simulations, however, our improved method covers time windows from which all dynamical scales including the relaxation rate can be extracted. Thus, we use the exact PIMC data to determine and verify a sequential transfer model and, based on this procedure, obtain a complete understanding of the dynamical features of incoherent ET in DBA structures.

The paper is organized as follows. We briefly outline the model for describing dissipative ET dynamics in Sec. II and in Sec. III the corresponding real-time

---

\*email: lothar.muehlbacher@physik.uni-freiburg.de

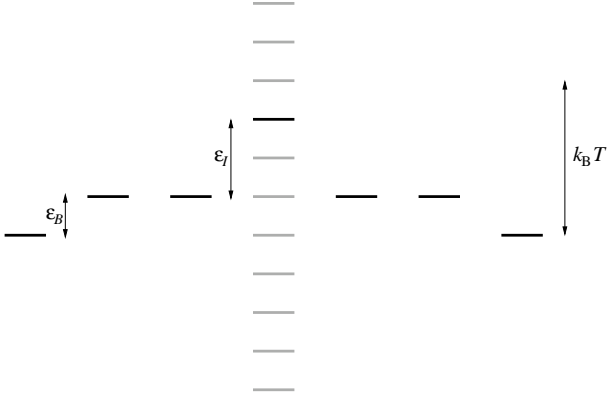


FIG. 1: Molecular chain with  $b = 5$  bridge states ( $d = 7$ ) and an impurity in its center. Gray bars denote the different energetic layouts for the impurity investigated in this paper.

PIMC simulation approach; for further details we refer to our previous paper Ref. [I]. Then, the numerical results are presented in Sec. IV, where we start in Sec. IV A by extracting intersite hopping rates from the PIMC data based on a sequential hopping model. The long time dynamics according to these findings is analysed in Sec. IV B and the dynamics of the total bridge compound in Sec. IV C. At the end a short summary and some conclusions are given.

## II. DYNAMICS OF THE DISSIPATIVE $d$ -LEVEL SYSTEM

We investigate the dynamics of a single electron moving on an impurity flawed molecular chain. The general approach to describe single charge transfer across bridges has been outlined in Ref. [I]. Here, we thus collect only the key ingredients. The molecular chain consists of  $d = 2S + 1$  discrete sites (see Fig. 1), where, separated by equal distances  $a$ ,  $b = d - 2$  adjacent bridge states  $\{|B_1\rangle, \dots, |B_b\rangle\}$  are clamped between a donor  $|D\rangle$  and an acceptor state  $|A\rangle$ . The latter two are energetically degenerated and define the 0-energy level. The bare bridge states are also energetically degenerated but at a higher energy  $\hbar\epsilon_{B_i} = \hbar\epsilon_B = 2.5\hbar\Delta$ , while the impurity, located in the center of the bridge  $|I\rangle = |B_{(d+1)/2}\rangle$ , exhibits an energy gap  $\epsilon_I = \epsilon_{B_{(d+1)/2}} - \epsilon_B$  with respect to the other bridge states (we only regard chains symmetric with respect to the impurity site, i.e. with an odd number of bridge sites). The focus of our study lies then on the transport across the bridge/impurity compound when this gap is energetically raised or lowered.

We restrict our model to nearest-neighbor coupling, that is, electronic motion is facilitated through tunneling which only occurs between adjacent states with a uniform real tunneling amplitude  $\Delta_{s,s'}$ . The electronic coordinate can then be expressed as

$$q(t) = a \cdot s(t), \quad (1)$$

where  $-S \leq s(t) \leq S$ . The position operator thus is equivalent to the spin  $S$  operator

$$a\mathbf{S}_z|s\rangle = as|s\rangle, \quad (2)$$

with  $|s\rangle$  denoting the (orthonormal) localized electronic states. In terms of electron transfer,  $|-S\rangle$  and  $|S\rangle$  represent the donor and acceptor  $|D\rangle$  and  $|A\rangle$ , respectively, while the other states are referred to as the bridge states.

The free  $d$ -level system ( $d$ LS) Hamiltonian can then be written as Ref. [I].

$$H_{dLS} = \hbar\mathbf{E}_z - \hbar\mathbf{S}_x, \quad (3)$$

where  $\mathbf{E}_z$  describes the energetic distribution of the electronic sites according to

$$\begin{aligned} \mathbf{E}_z|D\rangle &= \mathbf{E}_z|A\rangle = 0, \\ \mathbf{E}_z|B_i\rangle &= \epsilon_B|B_i\rangle \quad \text{for } 1 \leq i \leq b, \quad i \neq (d+1)/2, \\ \mathbf{E}_z|I\rangle &= (\epsilon_B + \epsilon_I)|I\rangle, \end{aligned} \quad (4)$$

while  $\mathbf{S}_x$  governs the tunneling,

$$\begin{aligned} \mathbf{S}_x|D\rangle &= \Delta|B_1\rangle, \\ \mathbf{S}_x|B_1\rangle &= \Delta(|D\rangle + |B_2\rangle), \\ \mathbf{S}_x|B_{(d+1)/2\mp 1}\rangle &= \Delta(|B_{(d+1)/2\mp 2}\rangle + |I\rangle), \\ \mathbf{S}_x|I\rangle &= \Delta(|B_{(d+1)/2-1}\rangle \\ &\quad + |B_{(d+1)/2+1}\rangle), \\ \mathbf{S}_x|B_i\rangle &= \Delta(|B_{i-1}\rangle + |B_{i+1}\rangle) \\ &\quad \text{for } i \in \{2, \dots, (d+1)/2 - 1, \\ &\quad (d+1)/2 + 1, \dots, d-1\}, \\ \mathbf{S}_x|B_b\rangle &= \Delta(|A\rangle + |B_{b-1}\rangle), \\ \mathbf{S}_x|A\rangle &= \Delta|B_b\rangle, \end{aligned} \quad (5)$$

The interaction with solvent and vibronic degrees of freedom is introduced within the framework of a system-plus-reservoir model, leading to the total Hamiltonian [10]

$$\begin{aligned} H &= H_{dLS} + H_I + H_B \\ &= H_{dLS} - a\mathbf{S}_z \sum_{\alpha} c_{\alpha} X_{\alpha} + (a\mathbf{S}_z)^2 \sum_{\alpha} \frac{c_{\alpha}^2}{2m_{\alpha}\omega_{\alpha}^2} \\ &\quad + \sum_{\alpha} \left( \frac{P_{\alpha}^2}{2m_{\alpha}} + \frac{1}{2}m_{\alpha}\omega_{\alpha}^2 X_{\alpha}^2 \right). \end{aligned} \quad (6)$$

Here, the residual degrees of freedom are archetypically modeled as a harmonic bath coupling bilinearly to the position of the electron ( $H_I$ ) [10]. As discussed in detail in Refs. [10, 21, 22], this provides a reasonably accurate description of reality for the great majority of ET systems.

For the dissipative electronic dynamics we focus on the *time-dependent site populations*,

$$P_{s_f, s_i}(t) = \text{Tr} \left\{ e^{iHt/\hbar} |s_f\rangle\langle s_f| e^{-iHt/\hbar} W_i(0) \right\}, \quad (7)$$

which are normalized,  $\sum_{s_f=-S}^S P_{s_f, s_i}(t) = 1$ , and where  $W_i(0)$  specifies the initial state of the total compound. In most theoretical and experimental works an initial separation of the electron and the environment is assumed corresponding to an initial density matrix

$$W_i(0) = Z_B^{-1} |s_i\rangle\langle s_i| e^{-\beta(H_B - s_i \mu \mathcal{E})}, \quad (8)$$

with the electron held fixed in state  $|s_i\rangle$  and the bath normalization  $Z_B = \text{Tr}\{e^{-\beta H_B}\}$  assuring the full system's density matrix to be normalized for all times. For a transfer process across the entire chain one typically prepares the electron initially in the donor state, i.e.  $|s_i\rangle = |D\rangle$  [11, 14]. Above,  $\mu$  is the dipole moment of the electron, and  $\mathcal{E}$  denotes the dynamical polarization of the bath [10], which is equilibrated with respect to the initial position of the electron. By comparing with Eq. (6), we see that  $\mu \mathcal{E} = a \sum_{\alpha} c_{\alpha} X_{\alpha}$ . As pointed out in Ref. [23], this “standard preparation” often used in ET experiments is especially suitable for a theoretical description of thermal transfer rates.

Switching to the path integral representation of Eq. (7), the bath degrees of freedom can be traced out exactly, yielding the reduced dynamics [10]

$$P_{s_f, s_i}(t) = \frac{1}{Z} \oint \mathcal{D}\tilde{s} \delta_{\tilde{s}(t), s_f} \exp \left\{ \frac{i}{\hbar} S_{dLS}[\tilde{s}] - \Phi[\tilde{s}] \right\}. \quad (9)$$

Here the path integration runs over closed paths  $\tilde{s}(t)$  starting at  $\tilde{s}(0) = s_i$  and propagating along the real-time contour  $t \in 0 \rightarrow t \rightarrow 0$ , which connect the forward and backward paths  $s(t')$  and  $s'(t')$ , respectively. Furthermore,  $S_{dLS}[\tilde{s}]$  denotes the total action of the free dLS. The influence of the traced-out bath is completely encoded in the *Feynman-Vernon influence functional*  $\Phi[s]$  [24],

$$\begin{aligned} \Phi[s, s'] &= \int_0^t dt' \int_0^{t'} dt'' [s(t') - s'(t')] [L(t' - t'') s(t'') \\ &\quad - L^*(t' - t'') s'(t'')] \\ &\quad + i \frac{\hat{\mu}}{2} \int_0^t dt' [s^2(t') - s'^2(t')] , \end{aligned} \quad (10)$$

which is written in terms of the complex-valued bath autocorrelation function reading for real time  $t$

$$\begin{aligned} L(t) &= \frac{1}{\hbar^2} \left\langle \left( \sum_{\alpha} c_{\alpha} X_{\alpha}(t) \right) \left( \sum_{\alpha} c_{\alpha} X_{\alpha}(0) \right) \right\rangle_{\beta} \\ &= \frac{1}{\pi} \int_0^{\infty} d\omega J(\omega) \frac{\cosh[\omega(\hbar\beta/2 - it)]}{\sinh(\hbar\beta\omega/2)} \end{aligned} \quad (11)$$

with  $\beta = 1/k_B T$  and

$$\hat{\mu} = \frac{2}{\pi} \int_0^{\infty} d\omega \frac{J(\omega)}{\omega} = 2\Lambda_{cl}. \quad (12)$$

Both quantities are completely determined by the spectral density

$$J(\omega) = \frac{\pi a^2}{2\hbar} \sum_{\alpha} \frac{c_{\alpha}^2}{m_{\alpha} \omega_{\alpha}} \delta(\omega - \omega_{\alpha}), \quad (13)$$

which for a condensed-phase environment typically becomes a continuous function of  $\omega$ . In the classical regime, the description of the bath reduces to the celebrated Marcus theory [8, 9], where the dissipative influence onto the electronic dynamics are fully governed by the classical *reorganization energy*  $\hbar\Lambda_{cl}$ .

### III. SIMULATION METHOD

We perform path-integral Monte Carlo (PIMC) simulations, utilizing a discretized version of the path-integral expression (9) where the electronic system's path  $s(t)$  is replaced by  $\{s_j\}_{1 \leq j \leq 2q}$ ,  $s_j = s((j-1)t/q)$ . The “dynamical sign problem” [25] notorious for real-time calculations of quantum systems is significantly relieved by employing an optimized filter based on the blocking approach which exploits certain symmetries of the influence functional [16]. Besides some improvements described below, we used the same computer code as described in detail in Ref. [1].

The computational bottleneck of this approach is the creation of the MC trajectory since the evaluation of each trial move requires the calculation of a series of matrix multiplications. However, here significant saving can be achieved. Starting with the standard MC weight,

$$\begin{aligned} w_{MC}(\{\xi_j\}, \eta_{q+1}) &\equiv \exp \left( - \sum_{k \geq j=2}^q \xi_k \Lambda_{k-j} \xi_j \right) \\ &\times \left| \left( \hat{K}^{(1)}(\xi_2, \dots, \xi_q) \cdots \hat{K}^{(q)}(\xi_q) \right)_{2s_i, \eta_{q+1}} \right|, \end{aligned} \quad (14)$$

where the exponential is the real part of the influence functional while the second factor represents a product of complex matrices, which include the complex valued contributions from the influence functional and the propagation of the undamped electronic system (for details, see Ref. [1] App. A), in a first step, these matrices are stripped off all dissipative terms leading to

$$\begin{aligned} \tilde{w}_{MC}(\{\xi_j\}, \eta_{q+1}) &\equiv \exp \left( - \sum_{k \geq j=2}^q \xi_k \Lambda_{k-j} \xi_j \right) \\ &\times \left| \left( \tilde{K}(0, \xi_2) \cdots \tilde{K}(\xi_q, 0) \right)_{2s_i, \eta_{q+1}} \right|. \end{aligned} \quad (15)$$

Now the matrices  $\tilde{K}(\xi_j, \xi_{j+1})$  can be computed from the free propagator alone and thus are, unlike the  $\hat{K}^{(j)}$  matrices in Eq. (14), *local in time* in the sense that they connect only two neighboring time slices. Accordingly, the former can be calculated and stored beforehand for all combinations of  $\xi_j$  and  $\xi_{j+1}$ , while the latter have to be recalculated every time a trial move is evaluated.

The respective speed up can be multiplied by computing and storing sequences of  $\tilde{K}$  matrices prior to performing the MC moves, e.g. with

$$\tilde{K}^{(n)}(\xi_1, \dots, \xi_{n+1}) \equiv \prod_{j=1}^n \tilde{K}(\xi_j, \xi_{j+1}), \quad (16)$$

which diminishes the number of matrix multiplications necessary to obtain  $\tilde{w}_{\text{MC}}$  by a factor of  $n$ . Of course this approach is limited by its memory consumption which increases exponentially with  $d$ . However, with the on-board memory facilities of nowadays computer's being in the GByte range, it still offers tremendous performance improvements in terms of simulation duration.

Finally, in a last step the  $\tilde{K}^{(n)}$  are replaced by real-valued matrices which are obtained from the former by replacing all matrix entries with their modulus. Similarly to ignoring the dissipative terms present in the original  $\tilde{K}^{(j)}$  matrices, this somewhat impairs the statistics of the PIMC simulation. However, in both cases the thus necessarily larger number of accumulation processes is more than compensated by the speed up of the evaluation of the trial moves, provided the system is not too far from the coherent-incoherent transition. Fortunately, far away from this transition the application of special techniques to soothe the sign problem usually is not necessary anyway. Note also that the deviation of the improved MC weight (15) from Eq. (14) decreases with increasing  $n$ .

To illustrate the effectiveness of this approach we performed calculations both with the improved as well as with the original MC weight. For the parameters used in this paper, the former achieved a speed up of typically a factor of 12; the data for  $\epsilon_I/\Delta = 5$  presented in Fig. 2, e.g., were obtained on IBM-P615 within a CPU time of 6.2 days with  $n = 4$  (cf. Eq. (16) and  $q = 100$  discretization steps on the real-time axis, where  $6.7 \times 10^7$  accumulation processes were performed; the statistical error in the average sign was 1.2%.

#### IV. TRANSFER DYNAMICS

For vanishing dissipation, the charge dynamics of an electron initially localized at the donor site displays coherent oscillations corresponding to no net-transfer to the acceptor site. These oscillations survive for weak coupling to an environment and sufficiently low temperatures, but with decreasing amplitude as the system relaxes towards its equilibrium state. In the sequel, we are interested in completely incoherent transport, where, however, quantum mechanical properties of the phonon bath play a substantial role and give rise e.g. to nuclear tunneling. According to our previous study, we consider a spectral density of the form

$$J(\omega) = 2\pi\alpha\omega e^{-\omega/\omega_c}, \quad (17)$$

where the damping strength is chosen as  $\alpha = 1/4$ , well below the coherent-incoherent transition  $\alpha \approx 1/2$ , and the cut-off frequency  $\omega_c/\Delta = 5$ . As seen in Ref. [I], for these parameters coherent oscillations in the electronic dynamics show up for  $\hbar\beta\Delta > 0.3$ . Therefore we fix the inverse temperature sufficiently above this transition at

$\hbar\beta\Delta = 0.1$ , which gives still rise to strong quantum effects in the bath ( $\omega_c\hbar\beta = 0.5$ ) though.

Following these lines, we expect an initial nonequilibrium state to decay – after an initial transient on a time scale  $\tau_{\text{trans}}$  – multi-exponentially towards thermal equilibrium. According to our previous simulations [I], the equilibrium occupation probabilities are taken to be Boltzmann distributed, i.e.,

$$\begin{aligned} P_D^\infty &= P_A^\infty = \frac{1}{2 + (b-1)e^{-\hbar\beta\epsilon_B} + e^{-\hbar\beta(\epsilon_B+\epsilon_I)}} \\ &= \frac{e^{\hbar\beta\epsilon_B}}{b-1 + 2e^{\hbar\beta\epsilon_B} + e^{-\hbar\beta\epsilon_I}}, \\ P_{B_i}^\infty &= \frac{1}{b-1 + 2e^{\hbar\beta\epsilon_B} + e^{-\hbar\beta\epsilon_I}}, \\ P_I^\infty &= \frac{e^{-\hbar\beta\epsilon_I}}{b-1 + 2e^{\hbar\beta\epsilon_B} + e^{-\hbar\beta\epsilon_I}}. \end{aligned} \quad (18)$$

Here,  $P_D^\infty, P_A^\infty, P_I^\infty$ , and  $P_{B_i}^\infty, i = 1, \dots, (d+1)/2-1, (d+1)/2+1, \dots, b$  denote the populations of donor, acceptor, impurity, and the remaining bridge sites, respectively, for  $t \rightarrow \infty$ . For intermediate to long times this decay is governed by a mono-exponential relaxation with a time constant that is the inverse of the total transfer rate  $\Gamma_T$ . The crucial question is then, to what extent signatures of the impurity can be detected in  $\Gamma_T$ , which often is the only observable accessible in experiments. In case that the molecular chain is connected to external leads being integrated into an electrical circuit, an applied dc-voltage gives rise to a steady state with a flux that is directly related to  $\Gamma_T$  [4].

##### A. Population dynamics and intersite hopping rates

For molecular chains with energetically degenerated bridge states, but variable length treated in Ref. [I], a sequential hopping model turned out to capture the population dynamics for times beyond the transient time scale quite well. Further, direct transfer populating bridge sites only virtually, known as superexchange, turned out to play no substantial role for the bath parameters specified above even for larger energy gaps between the intermediate and donor/acceptor sites. Consequently, we assume first a purely sequential model to be applicable also here which is self-consistently verified by analysing the QMC data. The influence of superexchange is included in a second step.

Then, the population dynamics for  $\mathbf{P} = (P_D, P_{B_1}, \dots, P_{B_b}, P_A)$  is governed by

$$\dot{\mathbf{P}} = \mathbf{A}\mathbf{P}, \quad (19)$$

with a rate matrix independent of time for  $t > \tau_{\text{trans}}$

$$A = \begin{pmatrix} -\Gamma_{DB} & \Gamma_{BD} & 0 & & & \dots & 0 \\ \Gamma_{DB} & -\Gamma_{BD} - \Gamma_B & \Gamma_B & 0 & & \dots & \\ 0 & \Gamma_B & -2\Gamma_B & \Gamma_B & 0 & \dots & \vdots \\ \vdots & & \ddots & \ddots & \ddots & \ddots & \\ & 0 & \Gamma_B & -\Gamma_B - \Gamma_{BI} & \Gamma_{IB} & 0 & \\ & & 0 & \Gamma_{BI} & -2\Gamma_{IB} & \Gamma_{BI} & 0 \\ & & & 0 & \Gamma_{IB} & -\Gamma_{BI} - \Gamma_B & \Gamma_B & 0 \\ & & & & \ddots & \ddots & \ddots & \ddots & \vdots \\ \vdots & \dots & & 0 & \Gamma_B & -2\Gamma_B & \Gamma_B & 0 & \\ 0 & & \dots & & \ddots & 0 & \Gamma_B & -\Gamma_B - \Gamma_{BA} & \Gamma_{AB} \\ & & & & & & 0 & \Gamma_{BA} & -\Gamma_{AB} \end{pmatrix} \quad (20)$$

Note that Eq. (19) can be derived from an exact non-local retarded Master equation [26]. Due to the sequential hopping, the intersite rates  $\Gamma_{DB}, \Gamma_{BD} = (P_B^\infty/P_D^\infty)\Gamma_{DB}$ , and  $\Gamma_B$  should be independent of the gap energy  $\hbar\epsilon_I$  of the impurity, as our simulations confirm (see below). The latter one determines only  $\Gamma_{BI}$  and  $\Gamma_{IB}$  which are related by the detailed balance condition

$$\Gamma_{BI} = \frac{P_B^\infty}{P_I^\infty} \Gamma_{IB} = e^{\pm \hbar\beta\epsilon_I} \Gamma_{IB}. \quad (21)$$

The intersite rates were then obtained from our QMC data by the following procedure: For increasing values of the transient time scale  $\tau_{\text{trans}}$  starting at  $\tau_{\text{trans}} = 0$ , the populations stemming from solving Eq. (19) with integration constants specified by the QMC results for  $P_A(\tau_{\text{trans}}), \dots, P_D(\tau_{\text{trans}})$  were fitted to the QMC data for  $P_A(t \geq \tau_{\text{trans}}), \dots, P_D(t \geq \tau_{\text{trans}})$ . This fixed the intersite rates as functions of the transient time scale. Each true rate constant then was extracted as the plateau value of its corresponding rate function with  $\tau_{\text{trans}}$  as the actual transient time. The rates were fitted in sequel rather than at once. First,  $\Gamma_{DB}$  and  $\Gamma_B$  were obtained from a fit to a completely degenerated bridge, i.e.  $\epsilon_I = 0$ , with  $\hbar\beta\Delta = 0.1$  and  $\epsilon_B = 2.5\Delta$ , yielding

$$\begin{aligned} \Gamma_{DB}/\Delta &= 0.298, \\ \Gamma_{BD}/\Delta &= 0.383, \\ \Gamma_B/\Delta &= 0.370, \end{aligned} \quad (22)$$

which basically coincide with the golden rule values, see Ref. [I], Eq. (22). For impurity bridges,  $\epsilon_I \neq 0$ , the bridge-impurity rate  $\Gamma_{BI}$  remains thus as the only parameter in the sequential population dynamics (19). A subsequent fit yields  $\Gamma_{BI}$  as a function of the impurity offset  $\epsilon_I$ . The existence of time independent intersite rates (plateau time) and the accuracy of this procedure proofs in turn the applicability of the hopping model.

We start by presenting as an example in Figs. 2, 3 PIMC data for the population dynamics of a bridge with

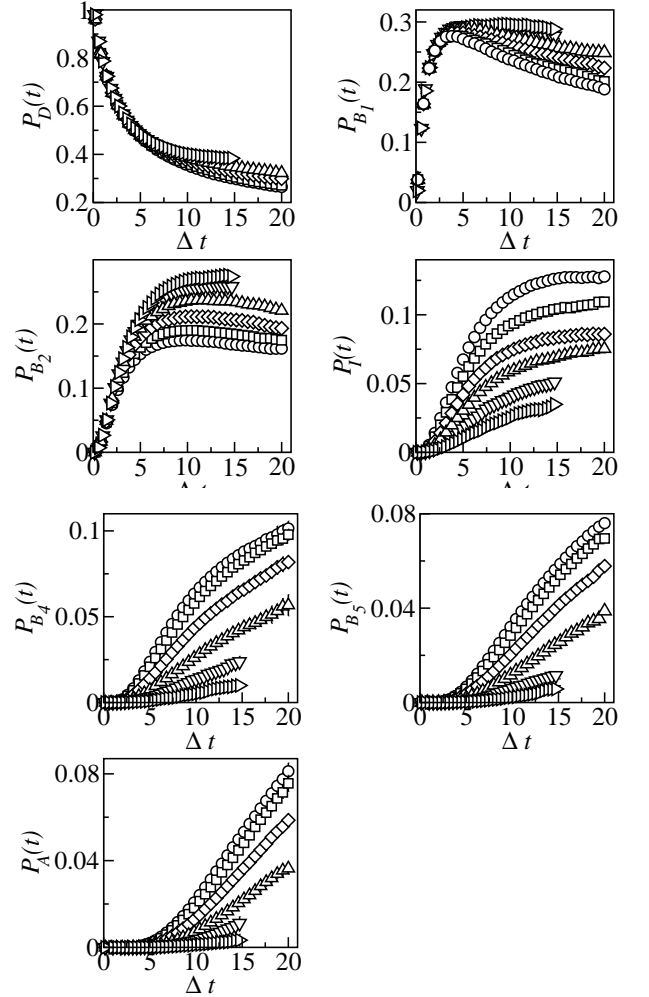


FIG. 2: Electronic populations for  $\alpha = 1/4$ ,  $\omega_c/\Delta = 5$ ,  $\hbar\beta\Delta = 0.1$ ,  $\epsilon_B/\Delta = 2.5$  and  $\epsilon_I/\Delta = 0, 2.5, 5, 7.5, 10$ , and  $12.5$  (circles, squares, diamonds, triangles up, triangles down, and triangles right, respectively).

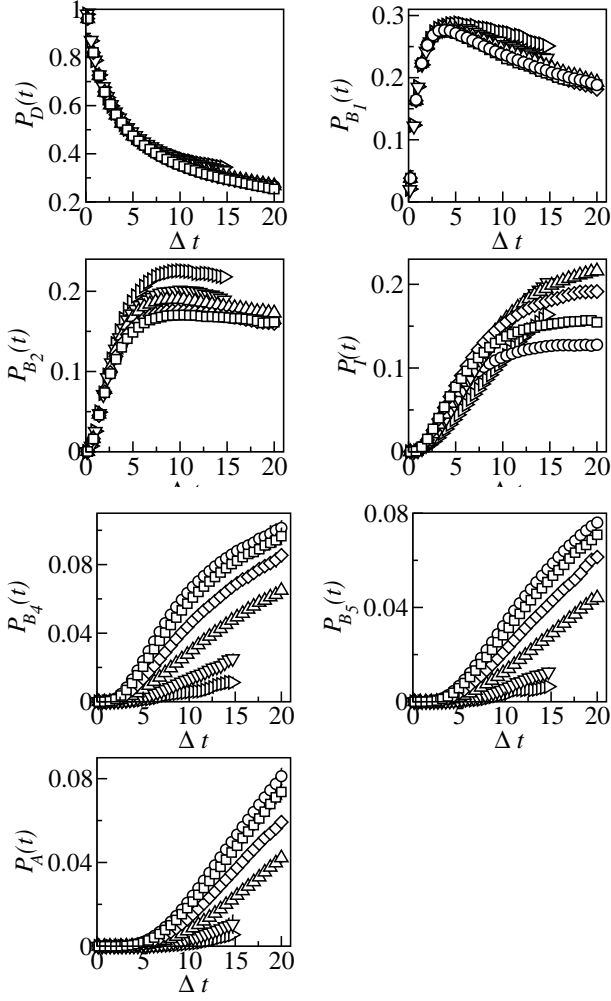


FIG. 3: Electronic populations for  $\alpha = 1/4$ ,  $\omega_c/\Delta = 5$ ,  $\hbar\beta\Delta = 0.1$ ,  $\epsilon_B/\Delta = 2.5$  and  $\epsilon_I/\Delta = 0, -2.5, -5, -7.5, -10$ , and  $-12.5$  (circles, squares, diamonds, triangles up, triangles down, and triangles right, respectively).

$d = 7$ . Our simulations included bridges with  $b = 3, 5, 7$  ( $d = 5, 7, 9$ ) and gap energies between  $-12.5 \leq \epsilon_I/\Delta \leq 12.5$  in steps of 2.5. To obtain rate constants with sufficient accuracy, the simulations had to be performed with exceptional small statistical error and up to long times  $\Delta t = 20$ . For example, for a typical coupling  $\Delta = 300 \text{ cm}^{-1}$  this corresponds to simulation times up to 60 ps. In Fig. 4 we display corresponding results for  $\Gamma_{BI}$  as a function of the energy gap  $\epsilon_I$ . Qualitatively, the numerical rates follow the golden rule formula, but deviate, as expected, from the classical Marcus expression [see Ref. [1], Eq. (21)]. Quantitatively, however, they are smaller than the golden-rule results by about 10% or less, a fact that can partly be attributed to adiabatic effects like recrossings in the Landau-Zener region since our bath is not strictly in the nonadiabatic limit where the golden rule expression is valid. Rates for different bridge lengths differ by less than 2% outside the maximum and by about 5% at the maximum where those

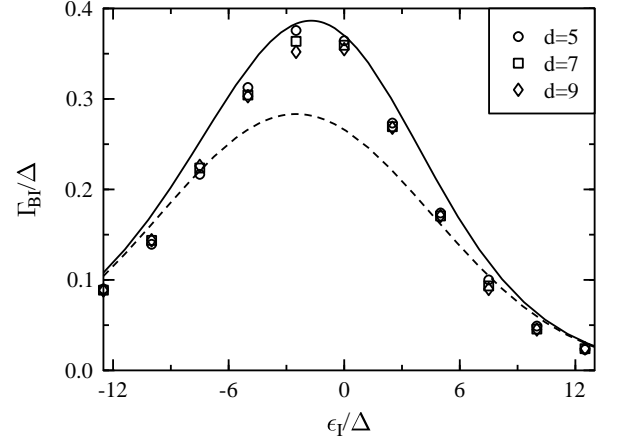


FIG. 4: Bridge-impurity rate  $\Gamma_{BI}$  as a function of the impurity energy gap  $\epsilon_I$ . Rates extracted from PIMC simulations (markers) for various chain length with  $d = 5, 7, 9$  are shown together with the results according to the classical Marcus (dashed) and the quantum mechanical golden rule (solid) expressions.

for shorter bridges exceed those of longer ones. In the classical limit, the pronounced maximum of  $\Gamma_{BI}(\epsilon_I)$  corresponds to an activationless transfer at  $\epsilon_I = -\Lambda_{cl}$ , while for  $\hbar\beta\omega_c \geq 1$  collective quantum effects in the bath promote nuclear tunneling between adiabatic surfaces, shifting its location towards smaller gap energies (cf. fig. 4). Note that  $\Gamma_{BI} > \Gamma_B$  around the maximum. Deviations between rates for different  $b$  are the largest close to this maximum where adiabatic effects are expected to be the strongest as the bath is directly located around the transition point.

The non-monotonic behavior of  $\Gamma_{BI}(\epsilon_I)$  is already well-known from Marcus theory since the activation barrier between bridge and impurity state is a quadratic function of  $\epsilon_I + \Lambda$ , see Ref. [1], Eq. (21). Therefore, Marcus rates show perfect symmetry with respect to  $\epsilon_I = -\Lambda = -2.5\Delta$ . The fact that acceptor populations in Fig. 2 and 3, however, exhibit a symmetric behavior with respect to  $\epsilon_I = 0$ , simply reflects the symmetry properties of the total rate  $\Gamma_{BI}(\epsilon_I) + \Gamma_{IB}(\epsilon_I) = \Gamma_{BI}(\epsilon_I) + \Gamma_{BI}(-\epsilon_I)$ . For long times, of course this symmetry in the  $P_A(t)$  is broken due to the different equilibrium populations.

Based on these results and Eq. (19), we show in Fig. 5 populations  $P_D(t)$  and  $P_I(t)$  for  $b = 5$  at fixed times but for varying  $\epsilon_I$ . This gives deeper insight in how the final equilibrium populations (18) are established during the time evolution. Namely, the impurity population tends to establish an exponential dependence  $\propto \exp(-\hbar\beta\epsilon_I)$  on a much shorter time scale than the donor one displays a behavior  $\propto \exp[\hbar\beta(\epsilon_B + \epsilon_I)]$ . We will see in detail below that this is a characteristic facet of the DBA dynamics.

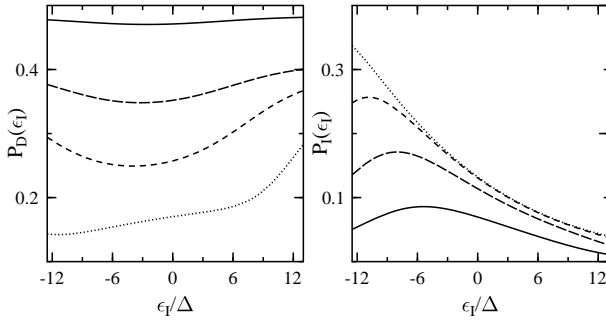


FIG. 5: Donor population  $P_D$  (left) and impurity population  $P_I$  (right) for  $d = 7$  at fixed times vs.  $\epsilon_I$ . Left:  $\Delta t = 5$ , (solid), 10 (long-dashed), 20 (short-dashed), 100 (dotted); right:  $\Delta t = 5$ , (solid), 10 (long-dashed), 20 (short-dashed), 50 (dotted).

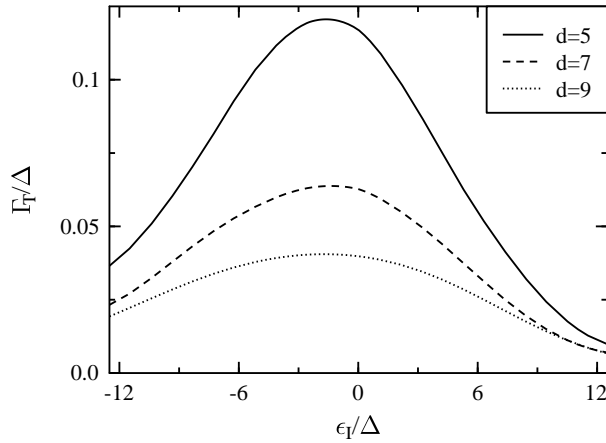


FIG. 6: Total transfer rate  $\Gamma_T$  according to the intersite hopping rates extracted from the PIMC simulations and the rate dynamics Eq. (19) for molecular chains with  $d = 5, 7, 9$  sites vs. the impurity gap  $\epsilon_I$ .

### B. Total transfer rate

With  $\Gamma_{IB}$  at hand, the transfer dynamics according to Eq. (19) is known for arbitrary times. In particular, the least non-vanishing eigenvalue of the rate matrix  $A$  defines the total transfer rate  $\Gamma_T$  being typically, e.g. for longer bridges, much smaller than the intersite rates. This way, we get access to information in the extreme long time range by extracting intersite rates from exact PIMC simulations.

Results are depicted in Fig. 6 for varying gap energy  $\epsilon_I$  and bridge lengths  $b = 3, 5, 7$ . As discussed, the overall values of  $\Gamma_T$  are smaller by about a factor of 5 to 10 compared to the intersite hopping rates meaning that the time scales for local dynamics are well separated from global relaxation. Strikingly, there is a maximum at  $\epsilon_I/\Delta \approx -1.5$  which is a signature of the activationless regime found in the  $\Gamma_{BI}$  rate. Hence, a defect with an appropriate negative gap enhances the global transport dynamics compared to the situation where it is absent.

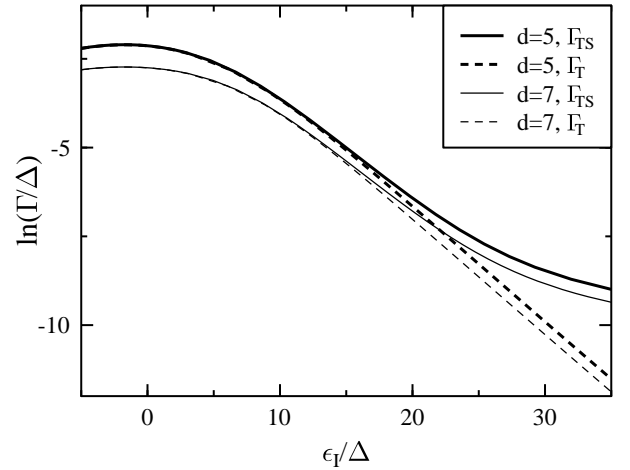


FIG. 7: Total transfer rates without ( $\Gamma_T$ , dashed) and including superexchange across the impurity site ( $\Gamma_{TS}$ , solid) vs.  $\epsilon_I$ .

Of course, for very large negative and positive gaps the chain is basically cut into pieces and the sequential transfer to the acceptor tends to vanish.

In our previous studies, non-sequential electronic transport processes (superexchange) played only a minor role. For the range of gap energies considered in the PIMC simulations, the same holds true here. Since the rates gained from the PIMC data are close to the golden rule rates, particularly for higher/lower impurity sites, we analyse the situation for extreme gap energies by additionally including direct transfer without populating the impurity, i.e. from  $|B_{(d+1)/2-1}\rangle$  to  $|B_{(d+1)/2+1}\rangle$ , into the rate matrix  $A$  via a superexchange rate  $\Gamma_{SE}$ . Knowing that superexchange is relevant for high lying impurities only, we estimate  $\Gamma_{SE}$  from a quantum mechanical golden rule expression as well (fourth order perturbation theory in  $\Delta$ ), see Eqs. (23), (25) in Ref. [1]. The corresponding  $\Gamma_{TS}(\epsilon_I)$  is shown together with  $\Gamma_T$  in Fig. 7 and verifies that for the total transfer, sequential hopping dominates by far up to impurities with  $\epsilon_I/\Delta \leq 20$ . Superexchange dominates for larger gaps though, where the transport to the acceptor is almost frozen. In this latter regime *electronic tunneling* through the impurity exceeds the effect of *nuclear tunneling* in the sequential hopping mechanism.

### C. Bridge relaxation

Even though the molecular bridge including the defect plays a key role in the charge transfer from donor to acceptor, typically in experiments individual bridge site populations are not accessible. Thus, the question arises whether the bridge compound considered as a sub-unit of the entire molecular DBA structure exhibits a characteristic dynamics on its own. For that purpose, we look at the total bridge population  $P_B = \sum_l P_{B_l}$  where the sum

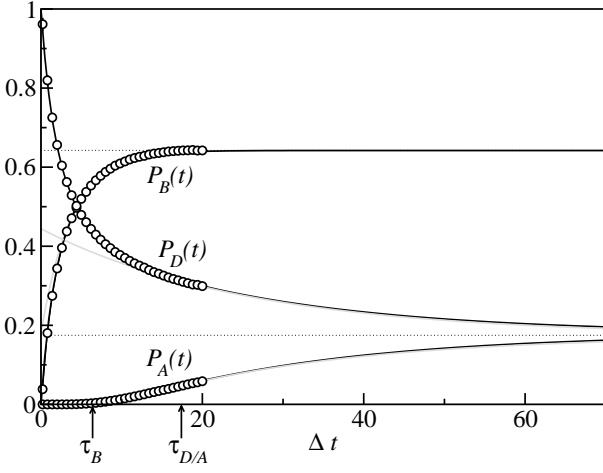


FIG. 8: Time dependent populations of bridge  $P_B(t)$ , donor  $P_D(t)$ , and acceptor  $P_A(t)$  for a bridge with  $b = 5$  sites and an impurity gap  $\epsilon_I/\Delta = 5$ . Dots represent PIMC data, solid lines the full population dynamics according to Eq. (19), and grey lines the asymptotic behavior according to Eqs. (23) and (24), see text. The dotted lines indicate the equilibrium populations.

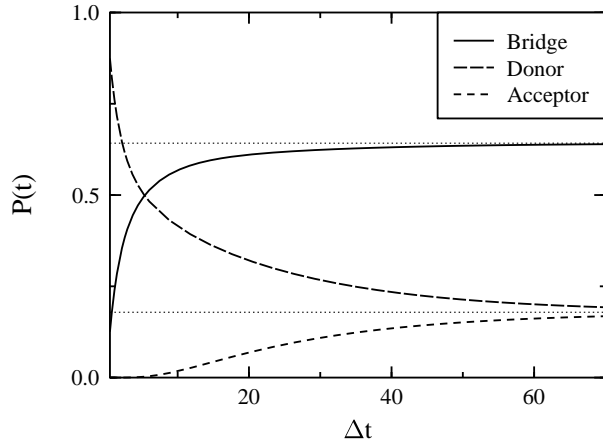


FIG. 9: Time dependent populations of bridge  $P_B(t)$ , donor  $P_D(t)$ , and acceptor  $P_A(t)$  for a bridge with  $b = 5$  sites and an impurity gap  $\epsilon_I/\Delta = 5$  where the impurity is located one site to the left of the center of the bridge. Dotted lines indicate the respective equilibrium values.

runs over all bridge sites including the impurity. Clearly, due to normalization  $P_B = 1 - P_D - P_A$ .

Upon closer inspection one finds that due to the symmetry of the rate matrix in Eq. (19), every second term in  $P_B(t)$  drops out exactly so that its asymptotic dynamics is governed by the second least eigenvalue of  $A$ , denoted by  $\Gamma_{TB}$ , instead of  $\Gamma_T$ . For times beyond a certain threshold  $\tau_B \ll 1/\Gamma_T$ , the bridge saturation can thus be captured by

$$P_B(t) = P_B^\infty + [P_B(\tau_B) - P_B^\infty]e^{-\Gamma_{TB}(t-\tau_B)} \quad (23)$$

where  $\Gamma_{TB} \gg \Gamma_T$ ; accordingly, even if the intersite rates in  $A$  are not known,  $\Gamma_{TB}$  can still be found by study-

ing the saturation limit of the time dependent expression  $\Gamma_{TB}(t) = \dot{P}_B(t)/|P_B(t) - P_B^\infty|$ . This theoretical prediction from the hopping model is completely verified by the simulations as shown in Fig. 8, where  $P_B(t)$  for fixed gap  $\epsilon_I/\Delta = 5$  is depicted as a function of time. Apparently, it tends to saturate on a considerably smaller time scale than the total chain relaxes towards thermal equilibrium. An explicit value for the transient time  $\tau_B$  is gained from the condition that the actual  $P_B(t)$  and its asymptotics (23) differ by less than 1%. This leads to  $\Delta\tau_B = 6.4$  which is considerably below the simulation time. As seen in Fig. 10, the bridge relaxation rate takes its maximum not at negative, but rather positive gap energies, where the overall transfer is slowed down. In this case, the defect facilitates as a scattering center first relaxation to its left side and then to its right one by blocking the flux to the acceptor site. Note again that the asymptotic dynamics (23) of the total compound does not mean that the *individual* bridge site populations have approached their equilibrium values, too.

Now, for very long times  $t \gg 1/\Gamma_{TB}$  one has  $\dot{P}_D(t) = -\dot{P}_A(t)$  so that then the transport across the DBA complex can be described within an effective two state model with a transfer rate being identical to the total transfer rate  $\Gamma_T$  extracted above, i.e.,

$$\begin{aligned} P_D(t) &= P_D^\infty + [P_D(\tau_{D/A}) - P_D^\infty]e^{-\Gamma_T(t-\tau_{D/A})} \\ P_A(t) &= P_D^\infty - [P_D(\tau_{D/A}) - P_D^\infty]e^{-\Gamma_T(t-\tau_{D/A})} \end{aligned} \quad (24)$$

Here, besides  $\Gamma_T$  only information about the donor enters. Further,  $\Delta\tau_{D/A} = 17.4$  (extracted similar as described above for  $\tau_b$ ) obeys  $\tau_{D/A} \gg 1/\Gamma_{TB}$  and lies also well within the simulation time window, thus verifying that the PIMC simulations cover the entire relevant time range. Everything beyond this range is in a sense "simple" and completely determined by the information retrieved from the numerical data. The comparison between Figs. 6 and 10 reveals that indeed  $\Gamma_{TB} \gg \Gamma_T$ .

While this strong time separation is no longer true for a defect located off center, the total bridge population comes still significantly closer to its equilibrium value on a time scale much below  $1/\Gamma_T$  than  $P_D$  and  $P_A$ , see Fig. 9. The remaining deviation falls off with  $\Gamma_T$ , but practically Eq. (24) still gives an accurate description of the D-A transfer at long times. Hence, the underlying scenario for the DBA transfer is this: On an intermediate time scale  $1/\Gamma_{TB}$  a local steady state for the total bridge population is established, which then acts for larger times merely as an electronic reservoir mediating between D and A. In turn, the comparison between the dynamics of  $P_A(t) + P_D(t)$  and the individual populations  $P_D(t)$ ,  $P_A(t)$  would allow experimentally to gain information about the symmetry of the bridge/defect structure. In this context it is worthwhile to mention that a symmetric situation treated here numerically is not just an idealized toy model but can actually be realized in experiments, see Ref. [20].

The above findings on the time scale separation allow for a simple recipe to successively extract rate constants



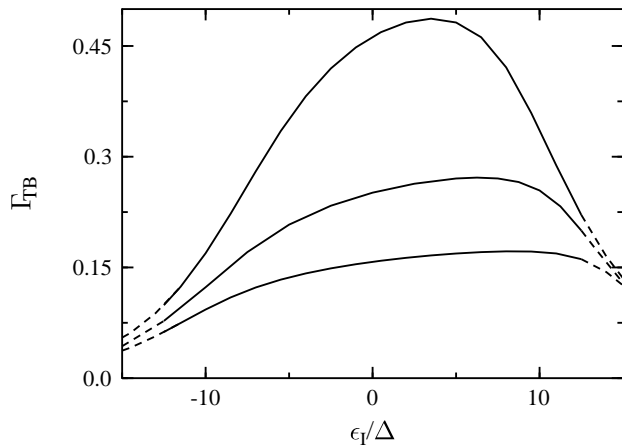


FIG. 10: Bridge relaxation rate  $\Gamma_{TB}$  vs.  $\epsilon_I$  for bridges with  $b = 3, 5, 7$  (from top to bottom), see text for details. The solid lines are based on the PIMC data, while for  $|\epsilon_I/\Delta| > 12.5$  the dashed lines are extrapolations based on golden rule hopping rates to better see the fall-off.

from the donor and acceptor dynamics only. Namely, in a first step  $\Gamma_T$  is obtained from the asymptotic behavior of  $P_D(t)$  and  $P_A(t)$ . Then, for a symmetric system  $P_D(t) + P_A(t)$  allows to obtain the second least rate constant  $\Gamma_{TB}$ . Further, by subtracting the dynamics corresponding to these rates from  $P_D(t)$  and  $P_A(t)$  the third least eigenvalue shows up etc. Practically, this procedure works for the rate constants governing the dynamics from moderate to long times for which typically a sufficient separation of time scales is guaranteed.

## V. SUMMARY AND CONCLUSIONS

Based on a recently improved real-time QMC scheme to treat numerically exact electronic transfer dynamics in condensed phase, we analysed the impact of an impurity on transport across molecular chains. Experimentally, this is not only the typical situation in native structures, but advanced molecular synthesis even allows to assemble corresponding chains in a controlled way. We restricted our study to the case of an impurity site with an energy gap to its neighboring sites, which can be seen as the archetypical scenario as it provides e.g. also an effective

description of a defect in the electronic intersite coupling.

Our main focus was the total transfer rate corresponding to the time scale for global relaxation towards thermal equilibrium. Since for longer bridges this time scale is in general considerably larger than the largest times accessible in real-time PIMC simulations, we used the latter ones to extract, beyond a transient time, intersite hopping rates between the electronic sites. This information was then used in a sequential transfer model, verified by the PIMC data, to capture the extreme long time dynamics.

Roughly, two dynamical ranges can be distinguished in the charge transfer: In a first step, the total bridge population approaches (symmetric bridge/defect) or comes close to (asymmetric bridge/defect) its value for thermal equilibrium facilitated by the presence of an impurity, while in a second step overall relaxation sets in associated with a characteristic unique time scale, the total transfer rate. Even though the total bridge population tends to saturate in the first range, intersite relaxation between individual sites still takes place. Nevertheless, the bridge compound including the impurity can basically be treated as a thermal reservoir mediating the transfer from donor to acceptor. The extent to which a time scale separation between bridge and total relaxation can be observed is directly related to the bridge/defect symmetry. The total transfer rate exhibits a pronounced maximum at negative values of the impurity energy gap, thus reflecting the enhancement of the local bridge-impurity rate in or near the activationless regime. In principle, a controlled doping with a defect site may therefore accelerate the transfer across a degenerated chain. As in our previous study, superexchange across the impurity plays a dominant role for extremely large gaps where the transport comes almost to rest. Our analysis may give qualitative and quantitative insight into experiments similar to the one reported in Ref. [20] where a molecular chain contacted with leads was designed to include a defect at its center.

## Acknowledgments

We acknowledge financial support from the DFG through Grant No. AN336-1 and the Landesstiftung Baden-Württemberg gGmbH. J.A. is a Heisenberg fellow of the DFG.

- 
- [1] J. Jortner and M.A. Ratner (eds.), *Molecular Electronics*, (Blackwell Sci., Oxford, 1997).
  - [2] J. Jortner and M. Bixon, eds., *Adv. Chem. Phys.* **106**, 107 (1999).
  - [3] C. Dekker and M.A. Ratner, *Phys. World* **14**, 29 (2001).
  - [4] A. Nitzan, *Ann. Rev. Phys. Chem.* **52**, 681 (2001).
  - [5] P. Hänggi and M.A. Ratner (eds.), *Chem. Phys.* **281**, (2002).
  - [6] C. Kergueris, J.-P. Bourgoin, S. Palacin, D. Esteve, C. Urbina, M. Magoga, and C. Joachim, *Phys. Rev. B* **59**, 12505 (1999).
  - [7] J. Reichert, R. Ochs, H.B. Weber, M. Mayor, and H.v. Löhneysen, *Appl. Phys. Lett.* **82**, 4137 (2003).
  - [8] R.A. Marcus, *J. Chem. Phys.* **24**, 966 (1956).
  - [9] R.A. Marcus and N. Sutin, *Biochim. Biophys. Acta* **811**, 265 (1985).

- [10] U. Weiss, *Quantum Dissipative Systems*, Series in Modern Condensed Matter Physics, Vol. 2 (World Scientific, Singapore, 1998).
- [11] A.K. Felts, W.T. Pollard, and R.A. Friesner, J. Phys. Chem. **99**, 2929 (1995).
- [12] A. Okada, V. Chernyak, and S. Mukamel, J. Phys. Chem. A **102**, 1241 (1997).
- [13] W.B. Davis, M.R. Wasielewski, M. Ratner, V. Mujica, and A. Nitzan, J. Phys. Chem. **101**, 6158(1997).
- [14] D. Segal, A. Nitzan, W.B. Davis, M.R. Wasielewski, and M.A. Ratner, J. Phys. Chem. **104**, 3817 (2000).
- [15] L. Mühlbacher, J. Ankerhold, and C. Escher, J. Chem. Phys. **121**, 12696 (2004).
- [16] C.H. Mak and R. Egger, Adv. Chem. Phys. **93**, 39 (1996).
- [17] M. Magoga and C. Joachim, Phys. Rev. B **56**, 4722 (1997).
- [18] W.B. Davis, W.A. Svec, M.A. Ratner, and M.R. Wasielewski, Nature **396**, 60 (1998).
- [19] B. Giese, J. Amaudrut, A.-K. Köhler, M. Spormann, and S. Wessley, Nature **412**, 318 (2001).
- [20] M. Mayor, C. von Hänisch, H.B. Weber, J. reichert, D. Beckmann, Angew. Chemie **41**, 1183 (2002).
- [21] D. Chandler, in *Liquids, Freezing and the Glass Transition*, ed. by D. Levesque, J.P. Hansen. and J. Zinn-Justin (Elsevier Science, North Holland, 1991), Les Houches 51, Part 1.
- [22] X. Song and A.A. Stuchebrukhov, J. Chem. Phys. **99**, 969 (1993).
- [23] L. Mühlbacher and R. Egger, J. Chem. Phys. **118**, 179 (2003).
- [24] R.P. Feynman and F.L. Vernon, Ann. Phys. (N.Y.) **24**, 118 (1963).
- [25] *Quantum Monte Carlo Methods in Condensed Matter Physics*, M. Suzuki (ed.) (World Scientific, Singapore, 1993), and references therein.
- [26] R. Egger, C.H. Mak, and U. Weiss, Phys. Rev. E **50**, (655)(R) (1994).